Title Page

Title: Pyroptosis-associated molecular classification and prognostic signature in glioma

Running head: Pyroptosis and glioma

Authors and affiliations

Lin Shen[1#], Yanyan Li[2#], Na Li[1], Yajie Zhao[3], Qin Zhou[1], Liangfang Shen[1], Zhanzhan Li[1*]

[#] These authors contributed equally to this work.

1. Department of Oncology, Xiangya Hospital, Central South University, Changsha, Hunan Province 410008, China.

2. Department of Nursing, Xiangya Hospital, Central South University, Changsha, Hunan Province 410008, China.

3. Department of Nuclear Medicine, Xiangya Hospital, Central South University Changsha, Hunan Province 410008, China.

***Correspondence to:** Zhanzhan Li, No.87, Xiangya Road, Kaifu District, Changsha, Hunan Province 410008, China. **E-mail:** lizhanzhan@csu.edu.cn

Disclosure of Potential Conflicts of Interest: The authors report no financial interests or relationships with the commercial sponsors of any products discussed in this report

Acknowledgments

This work was partly supported by the National Natural Science Foundation of China (ZL: No. 82003239), Science Foundation of Xiangya Hospital for Young Scholar (ZL:

NO. 2018Q012), and Hunan Province Natural Science Foundation (Youth Foundation Project) (ZL: NO. 2019JJ50945).

Word Count: Abstract: 244**; Text** 4992**; Tables** 0**; Figures** 6**; Supplementary materials:** Table :12, Figure:16; **References:** 42

Translational relevance describing

Few studies have investigated the role of pyroptosis in glioma, and comprehensive analyses of pyroptosis regulators in glioma, their correlation with clinical characteristics and their prognostic value have not been reported.The present study indicated that pyroptosis-related genes can be used to classify glioma patients into two subclasses based on different molecular features and clinical characteristics. The established prognostic model based on 15 pyroptosis-related genes not only predicted the prognosis of glioma patients but also reflected the molecular alterations, immune infiltration statuses, and stem cell-like properties of different risk groups. The classification based on the risk score of prognostic signature genes revealed a lncRNA-miRNA-mRNA regulatory network. The correlation of signature genes with drug sensitivity may provide a rationale for clinical applications. Finally, our study provides a new understanding of pyroptosis in the development and progression of glioma and contributes new important insights for promoting glioma treatment strategies.

Abstract

Purpose: Integrative analysis was performed in the Chinese Glioma Genome Atlas and The Cancer Genome Atlas to describe the pyroptosis-associated molecular classification and prognostic signature in glioma.

Experimental Design: Pyroptosis-related genes were used for consensus clustering and to develop a prognostic signature. The immune statuses, molecular alterations and clinical features of differentially expressed genes were analyzed among different subclasses and risk groups. A lncRNA-miRNA-mRNA network was built, and drug sensitivity analysis was used to identify small molecular drugs for the identified genes.

Results: Glioma can be divided into two subclasses using 30 pyroptosis-related genes. Cluster 1 displayed high immune signatures and poor prognosis as well as high immune-related function scores. A prognostic signature based on 15 pyroptosis-related genes of the CGGA cohort can predict the overall survival of glioma and was well validated in the TCGA cohort. Cluster 1 had higher risk scores. The high-risk group had high immune cell and function scores and low DNA methylation of pyroptosis-related genes. The differences in pyroptosis-related gene mutations and somatic copy numbers were significant between the high-risk and low-risk groups. The ceRNA regulatory network uncovered the regulatory patterns of different risk groups in glioma. Nine pairs of target genes and drugs were identified.

Conclusions: Pyroptosis-related genes can reflect the molecular biological and

clinical features of glioma subclasses. The established prognostic signature can predict prognosis and distinguish molecular alterations in glioma patients. Our comprehensive analyses provide valuable guidelines for improving glioma patient management and individualized therapy.

Introduction

Gliomas are the most common types of primary tumors in the central nervous system and one of the most devastating tumors(1). At present, the main treatment methods of glioma are surgical resection, radiotherapy, chemotherapy or chemoradiotherapy(4). Although great efforts have been made to improve glioma treatment, the prognosis of glioma patients remains poor(5). One of the main reasons is that the molecular mechanism is still not fully understood. Therefore, the exploration and research of the underlying mechanism of gliomas and identification of potential treatment targets followed by application in clinical practice have important theoretical and practical significance.

Pyroptosis is one of the pathways involved in programmed cell death, such as apoptosis, ferroptosis, necroptosis, and autophagy(6). Cookson et al. first used pyroptosis to describe the caspase-1-dependent pattern of cell death found in macrophages(7). Pyroptosis, distinct from apoptosis and necrosis, contributes to a range of human diseases as a new mechanism of cell death. Pyroptosis is a proinflammatory form of programmed cell death that is dependent on the activity of caspase acid-specific proteases(8). In the coupling of the amino-terminal and

carboxy-terminal linkers of gasdermin D (GSDMD) by caspases, the latter is displaced onto the membrane and perforated, inducing moisture penetration, cell swelling and the release of inflammatory factors, which is followed by pyroptosis(9). A previous study reported that pyroptosis plays an important role in immunity and diseases. In recent years, its role in tumorigenesis and cancer development has been studied comprehensively. Various regulators have been reported to be involved in the process of pyroptosis and play pivotal roles in the progression of tumors, such as hepatocellular carcinoma, lung cancer, and breast cancer(11-13). However, comprehensive analyses of pyroptosis regulators in glioma, their correlation with clinical characteristics and their prognostic value have not been reported.

In this study, we first outlined the molecular subtypes of gliomas based on pyroptosis-related genes in the TCGA dataset and described the clinical and molecular characteristics and immune status of each subclass. Then, we developed a prognostic signature of pyroptosis-related genes based on the TCGA cohort, validated this prognostic signature in the TCGA cohort. Furthermore, we explored the clinical and molecular patterns, including immune infiltration, somatic copy number alterations, mutations, and DNA methylation, and established a lncRNA-miRNA-mRNA regulatory network. Finally, we explored the correlation between small molecular drugs and the identified prognostic signature genes. Our comprehensive analyses provide new insight into the functions of pyroptosis in the initiation, development, and progression of glioma.

Materials and methods

Data source

We downloaded the genomic data and clinical data of glioma patients from the CGGA (http://www.cgga.org.cn/) and TCGA databases (https://portal.gdc.cancer.gov/). The copy number alteration threshold data, masked copy number segmentation data, and 450K DNA methylation data of glioma were also downloaded from the TCGA database. Additional gene-centric RMA-normalized gene expression profiles and drug response data of over 1000 cancer cell lines were accessed from the Genomics of Drug Sensitivity in Cancer (GDSC) database (https://www.cancerrxgene.org/downloads). Immune-associated data, including immune cells and immunophenoscores, were downloaded from TCIA (https://tcia.at/home). Thirty-three pyroptosis-related genes were defined from a previous publication and are provided in Table S1(15-18).

Identification of glioma subclasses

The pyroptosis-related genes identified were subsequently used in unsupervised class discovery. We first excluded some genes with a low median absolute deviation value (≤0.5) in the overall glioma patient samples. Consensus clustering provides quantitative and visual stability evidence derived from repeated subsampling and clustering. Consensus clustering can be used to perform an analysis when a negative expression value exists, which is different from nonnegative matrix factorization (NMF) clustering(19). This process was completed using the ConsensusClusterPlus R package. We identified the optimal clustering number visualizing consensus matrix, tracking plot, and cumulative distribution function plot. In addition, a T-distributed

stochastic neighbor embedding-based approach was used to validate the clustering in glioma patients.

Gene set variation analysis

To evaluate the pathway enrichment of each sample, we performed gene set variation analysis (GSVA) and estimated the gene set enrichment for glioma subclasses. The KEGG gene set was downloaded from the GSEA database. We calculated the enrichment scores for every sample using the GSVA R package. Differential analyses were performed between glioma subclasses. An absolute log2-fold change (FC)>0.1 and adjusted P value >0.05 were considered significant. The results were presented using the “heatmap” R package.

Development and validation of a prognostic signature

We developed a pyroptosis-related prognostic signature based on the CGGA training cohort. Univariate Cox regression was used to evaluate the prognostic roles of 30 pyroptosis-related genes. Twenty differentially expressed genes with P<0.05 were entered into LASSO Cox regression, which identified potential genes for the prognostic signature in the CGGA training cohort. Finally, a prognostic signature model based on 15 pyroptosis-related genes was developed. Then, we calculated the risk score for each sample of the CGGA and TCGA validation cohorts using the obtained regression coefficient in the CGGA training cohort. The CGGA and TCGA samples were divided into a high-risk group and a low-risk group based on the median risk score. Kaplan-Meier analyses were used to compare the overall survival curves of the high-risk and low-risk groups in the training and validation cohorts. Univariate

and multivariate Cox regression analyses were performed to identify whether the risk score was an independent prognostic factor in the training and validating cohorts. We also established a prognostic nomogram to evaluate the clinical value of the prognostic signature. Calibration analysis of the prognostic predictive value of the nomogram was carried out using the calibrated function of the "mis" package in CGGA and TCGA cohort.

Differential expression and functional enrichment analysis

To explore the different molecular patterns for each subclass or risk group, we performed differential expression analyses using the "limma" R package. |Log2FC|>1 and adjusted P value <0.05 were defined as significant differential expression levels. Gene Ontology and KEGG pathway analyses were performed using the "clusterProfiler" package.

Estimation of tumor stem cell-like properties and immune infiltration

We used single-sample gene set enrichment analysis (ssGSEA) to estimate the enrichment score of stem cell-like properties (RNAss, DNAss) and the TME (stromal score, immune score, and ESTIMATE score) in the TCGA cohort because the CGGA dataset did not provide such data. The immune-related cell and function scores were also calculated for each sample (downloaded from https://www.gsea-msigdb.org/). Differential expression analyses were performed between glioma subclasses and risk groups. The correlation coefficients were calculated between the 15 prognostic genes and stem cell-like properties and TME scores.

Somatic copy number alteration, mutation, and DNA methylation analysis

Based on the risk groups in the TCGA cohort, we compared the somatic copy number alteration, mutation, and DNA methylation levels between the high-risk and low-risk groups using the “limma” R package. The results are presented using a heatmap and box plot.

Construction of a ceRNA network

To further explore the transcriptome regulation network of different risk groups, we first performed differential expression analyses for mRNAs, lncRNAs and miRNAs between the high-risk group and the low-risk group. Then, we used Cytoscape version 3.8.2 to establish a lncRNA-miRNA-mRNA regulatory network.

Correlation between signature genes and drug sensitivity

To explore the correlation between small molecular drugs and the identified prognostic signature genes, Pearson correlation coefficients were calculated. $|R|>0.25$ and $P>0.05$ were considered significantly correlated.

Statistical analysis

For continuous variables, Student’s t test and one-way ANOVA were used to compare differences in two subgroups and more than two subgroups, respectively. For categorical variables, the chi-square test was used. The log-rank test was used to compare the survival curves of Kaplan-Meier analysis. The hazard ratio (HR) and 95% confidence interval (CI) of each gene and clinical parameters were calculated when univariate and multivariate Cox regression were applied. Time-dependent receiver operating characteristic model analysis was performed to calculate the area under the curve (AUC) using the “timeROC” package. All analyses were achieved using R

software version 4.0. A two-sided P value <0.05 was considered significant unless otherwise specified.

Results

Identification of glioma subclasses

The flow chart of the data analysis is presented in Figure 1A. From two CGGA RNA-seq datasets, we obtained 1018 samples of gene expression data and further identified 30 pyroptosis-related genes based on MAD>0.5. The gene symbols and descriptions of the 30 pyroptosis-associated genes used for classification are listed in Table S1. We first explored the interactions among these genes using PPIs (Figure 1B), and the PPI network indicated that CASP8, CASP4, CASP1, NLRP3, NLRP1 and NLRC4 are hub genes. The correlation circle plot of the 30 genes is presented in Figure 1C (red: positive correlation; green: negative correlation). We identified the optimal k value as 2 by estimating the comprehensive correlation coefficient. Therefore, we divided the glioma samples into two different subclasses: cluster 1 and cluster 2. For the optimal k value (k=2), the consensus matrix showed a relatively sharp and clear boundary, indicating stable and robust clustering (Figure 1D). To verify the subclass stability, we further performed t-sensitivity PCA and found that a two-dimensional t-sensitivity distribution supported subtype clustering (Figure 1E). The consensus clustering for each sample is listed in Table S2, and other consensus clustering is presented in Figure S1.

To explore the overall survival differences between the two clusters, we performed Kaplan-Meier analysis. In the CGGA cohort, the median survival time was

significantly shorter in cluster 2 than in cluster 1 (MST: 1.87 vs. 6.92 years, P<0.001, Figure 1F). This result indicated that the two subclasses had distinct prognostic patterns.

Correlation of glioma subclasses with pyroptosis-related genes

Two subclasses were obtained based on pyroptosis-related genes. To explore the pathway enrichment for the two subclasses, we performed GSVA by transforming the expression data from a gene-by-sample matrix to a gene set by two subclasses. Then, differential pathways were enriched in the two subclasses. Compared with cluster 1, the GSVA results indicated that cluster 2 had 182 kinds of significantly differential signaling pathways (Table S3). The upregulated pathways were associated with immune-related pathways, such as autoimmune, allograft rejection, graft versus host disease, primary immunodeficiency, antigen processing and presentation. Some signaling pathways, such as the cytosolic DNA sensing pathway, NOD-like receptor signaling pathway, Toll-like receptor signaling pathway, and metabolism-related pathways, were also significantly enriched. The significantly downregulated pathway was long-term potentiation (Figure 2A). A previous study found that EGFR signaling upregulates the surface expression of the GluN2B-containing NMDA receptor and contributes to long-term potentiation in the hippocampus(20). The NMDA receptor is involved in glioma progression(21).

Clinical characteristics and transcriptomes of glioma subclasses

We explored the correlation of subclasses with clinical characteristics (Figure 2B). Compared with patients in cluster 2 with a favorable prognosis, patients in cluster 1

tended to have GBM (P<0.001), WHO grade IV (P<0.001), a higher proportion of age >41 years, 1p19q non-codeletion status (P<0.001), and IDH wildtype status (P<0.001). Sex, PRS type and radiotherapy status were not associated with the molecular subclasses (P>0.05). For the pyroptosis-related genes except CASP9, significant differential expression was observed in the two clusters. Among these differentially expressed genes, all genes were upregulated in cluster 1 and downregulated in cluster 2 (Figure 2B). We also compared the differences in pyroptosis-related genes in patients with different histologies, grades, IDH mutation statuses, and 1p19q statuses. Compared with the LGG group, the GBM group had one upregulated gene (AIM2) and 21 downregulated genes (Figure S2A). Twenty-one DEGs were found for grade, and their expression increased with increasing WHO grade (P<0.005, Figure S2B). For IDH status, 25 DEGs were found (Figure S2C). Thirty pyroptosis-related DEGs were found for 1p191 status (Figure 2SD).

We further performed differential expression analysis between cluster 1 and cluster 2. A total of 392 DEGs were found, 18 genes were upregulated, and 372 genes were downregulated in cluster 2 (Table S4). GO and KEGG enrichment analyses were performed for all DEGs (Table S5 and Table S6). A total of 874 differentially expressed functions were enriched, including 709 biological processes, 95 cellular components and 70 molecular functions. The top 30 enrichment results are presented in Figure S3. Most of these functions were associated with immunity. In addition, 56 pathways were also identified in the KEGG analysis (Figure S4), and the top five pathways were phagosome, Staphylococcus aureus infection, tuberculosis,

complement and coagulation cascades, and human T-cell leukemia virus 1 infection.

Correlation of glioma subclasses with immune status

To explore the tumor heterogeneity between the two subclasses, we investigated the immune cell and immune function differences. Compared with cluster 2, cluster 1 had higher aDC, CD8+ T cell, DC, iDC, macrophage, mast cell, neutrophil, NK cell, pDC, T helper cell, Tfh cell, Th2 cell, TIL, and Treg levels (all $P<0.001$, Figure S5A). Similarly, cluster 1 had higher immune function scores than cluster 2, including APC coinhibition, APC costimulation, CCR, checkpoint, cytolytic activity, HLA, inflammation promotion, MHC class I, parainflammation, T cell coinhibition, type I IFN response and type II IFN response (all $P<0.001$, Figure S5B).

Development of a pyroptosis-related prognostic signature in glioma

Initially, we performed univariate Cox regression to identify the correlations of the 30 pyroptosis-related genes with OS (Figure S6A) in the CGGA cohort. In total, 20 pyroptosis-related genes were identified as associated with the overall survival of glioma patients. The Kaplan-Meier plot indicated that high expression of CASP3, CASP4, CASP5, CASP6, CASP8, ELANE, GSMAD, IL6, NLRP3, NOD1, NOD2, PLCG1, PRKACA, PYCARD, and SCAF11 was associated with poorer OS in glioma. Using 20 prognostic pyroptosis-related genes, we developed a prognostic signature by performing LASSO regression in the CGGA training cohort (Figure S6B and S6C). Fifteen of the 20 prognostic genes were used to develop the risk signature. We calculated the risk score for each sample using the regression coefficients of the 15 genes. Glioma patients with risk scores greater than the median value were divided

into a high-risk group, and the others were divided into a low-risk group. Compared with the low-risk group, the high-risk group was more likely to have GBM (P<0.001), a higher WHO grade (P<0.001), recurrence (P<0.001), older age (P<0.001), IDH wildtype status (P<0.001), 1p19q non-codeletion status (P<0.001), and a history of chemotherapy (P<0.001). The heatmap showed the association between the risk group and clinical parameters and differentially expressed genes of the high- and low-risk groups (Figure S6D). Furthermore, we found that glioma patients belonging to cluster 1 (Figure S4A), patients with a poor prognosis (Figure S7B), patients with GBM (Figure S7C), patients with WHO grade IV (Figure S7D), patients with 1p19q non-codeletion status (Figure S7E), and patients with IDH wildtype status (Figure S7F) had higher risk scores (all P<0.001).

The Kaplan-Meier analysis showed that the high-risk group had a significantly poorer OS than the low-risk group (Figure 3A, Figure 3B, and Figure 3C). Univariate Cox regression indicated that the risk score was positively associated with OS in glioma (HR=3. 105, 95% CI: 2.681–3.596, P<0.001, Figure 3D). Multivariate Cox regression suggested that the risk score was an independent unfavorable prognostic predictor in glioma (HR=1.685, 95% CI: 1.392–2.039, P<0.001, Figure 3E). In addition, PRS type, tumor grade, and age were positively associated with OS. However, chemotherapy, wildtype IDH status, and 1p19q status were negatively associated with OS in the CGGA training cohort. The PCA plot indicated that patients in different risk groups were separated into obviously different clusters (Figure 3F). Time-dependent receiver operating characteristic analysis was performed to evaluate the predictability of the

prognostic model. Our results showed that the AUCs at 1 year, 2 years, and 3 years were 0.717, 0.784 and 0.773, respectively. We further compared the OS status among different histology, IDH status, 1p19q codeletion status, and grade subgroups. The results showed that the OS of the high-risk group was still poorer than that of the low-risk group (Figure S8A-S8I, all P<0.001).

External validation of the pyroptosis-related prognostic signature in glioma

To further validate the prognostic value of the pyroptosis-related gene model, we also calculated the risk score of glioma patients in the TCGA cohort using the regression coefficients of the CGGA cohort. The Kaplan-Meier analysis indicated a significant correlation of the high-risk group with worse OS than the low-risk group (Figure 4A-4C). Univariate Cox regression showed that the risk score was significantly associated with OS in the TCGA cohort (HR=2.084, 95% CI: 1.890–2.297, P<0.001, Figure 4D). In multivariate Cox regression, the risk score was also an independent prognostic indicator (HR=1.425, 95% CI: 1.247–1.629 P<0.001, Figure 4E). The PCA plot validated the high- and low-risk distribution of all glioma patients based on the TCGA cohort. Furthermore, the AUCs of the risk score were 0.844 at 1 year, 0.863 at 2 years, and 0.874 at 3 years.

Prognostic prediction models

To further evaluate the clinical prediction value of the prognostic signature, we constructed a prognostic nomogram model based on multivariate Cox regression analysis that included all clinical parameters in the CGGA cohort (Figure S9A). The calibration curves indicated that the clinical nomogram model could precisely predict

the 1-year, 3-year and 5-year OS of glioma patients (C-index=0.799, Figure S9B-S9D). The predictive accuracy of this nomogram was well validated in the TCGA cohort (C-index=0.841, Figure S9E-S9G).

Functional enrichment and immune infiltration analyses based on the prognostic signature

We further explored the underlying biological functions that define the survival of glioma patients. We first performed DEG analysis between the high-risk and low-risk groups and then annotated the functions of the DEGs in terms of biological processes, cellular components, and molecular functions using GO enrichment and KEGG pathways. We identified 338 DEGs in the CGGA cohort (Table S7) and 2600 DEGs in the TCGA cohort (Table S8). The GO enrichment and KEGG pathway analyses indicated that the CGGA and TCGA cohorts shared some enrichment results, such as extracellular matrix organization, extracellular structure organization, immune response, ECM-receptor interaction, and cell adhesion molecules (Figure 5A-5D).

We also explored the differences in immune cells and immune functions based on the risk score in the CGGA (Figure 5E and Figure 5G) and TCGA datasets (Figure 5F and Figure 5H). As shown in the box plots, the immune cell score showed a similar trend in the CGGA and TCGA datasets. All immune cell scores were significantly upregulated in the high-risk group. The immune function differences of the different risk groups were the same in the CGGA and TCGA datasets (all $P<0.001$). All immune function scores were significantly upregulated in the high-risk group. Significant expression levels were also observed among different immune subtypes,

which indicated that the glioma prognosis risk could be associated with immune status (Figure S10). We also explored the correlation of the expression of target genes with cancer stem cell-like properties (RNAss, DNAss) and the TME (stromal score, immune score, and ESTIMATE score). We found that PCG1 was negatively associated with RNAss, the stromal score, the immune score, and the ESTIMATE score. SCAF11 was only negatively associated with DNAss. The rest of the genes showed positive correlations with RNAss, DNAss and the stromal, immune and ESTIMATE scores (Figure S11).

Molecular alterations of pyroptosis-related genes based on the prognostic signature

Molecular alterations of pyroptosis-related genes were also evaluated based on histology in the TCGA dataset. NLRP2, NLRP7, and PLCG1 were the only gene alterations in LGG, and NLRP3, NLRP7, NLRP2, SCAF11, NOD1, PLCG1, NLRP1, and CASP1 were gene alterations in GBM. All gene alterations were within 2% (Figure S12A and Figure S12B). The somatic copy number alteration analysis indicated significant differences among the pyroptosis-related genes. Among these genes, the copy variation number was significantly increased in GPX4, NLRP7, NLRP2, CASP3, CASP6, IL1B, CASP8, IL6, AIM2, NLRP4, NLRP3, PRKACA, ELANE, SCAF11, CASP9, NOD1, and PLCG1 and was significantly decreased in GSDMB, GSDMD, NLRP1, CASP9, TIRAP, CASP1, CASP4, NOD2, CASP5, PYCARD, GSMDC, GSMDA, and IL18 in the high-risk group (Figure S12C). The DNA methylation levels of the pyroptosis-related genes were also compared. The

results showed that the overall DNA methylation levels were significantly decreased in the high-risk group and increased in the low-risk group (Figure S12D).

Construction of a ceRNA network based on the prognostic signature

A ceRNA network was constructed based on the differentially expressed mRNAs, lncRNAs and miRNAs between the high-risk and low-risk groups in the TCGA dataset. We identified 763 downregulated mRNAs, 1176 upregulated mRNAs, 116 downregulated lncRNAs, 132 upregulated lncRNAs (Table S9), 47 downregulated miRNAs and 71 upregulated miRNAs (Table S10). Finally, 39 mRNAs (28 upregulated and 11 downregulated), 26 lncRNAs (15 upregulated and 15 downregulated) and 14 miRNAs (13 upregulated and 1 downregulated) were included in the ceRNA network (Figure 6). The Kaplan-Meier curves suggested that 13 lncRNAs (positive correlation: AC025211.1, AC068643.1, GDNF-AS1, and LINC00519; negative correlation: ADH1L1-AS2, CRNDE, FAM181A-AS1, HOTAIRM1, MCF2L-AS1, MIR210HG, NEAT1, SLC6A1, and SNHG9; Figure S13), 41 mRNAs (Figure S14 and Table S11) and 8 miRNAs (miR-21, miR-155, miR-200a, miR-216a, miR-221, miR-222, miR-429, and miR-503; Figure S15) were associated with OS in glioma patients.

Drug sensitivity analysis

To identify potential target drugs, we performed correlations of the identified prognostic signature genes with drugs. We identified 257 pairs of significant gene-drug correlations (Table S12). There were 9 pairs with correlation coefficients >0.5 or <-0.5.

ELANE-hydroxyurea, ELANE-cyclophosphamide, CASP3-nelarabine, NOD2-imiquimod, NLRP3-rebimastat, ELANE-ABT-199, ELANE-imexon, and NOD2-isotretinoin showed drug sensitivity. PRKACA-cobimetinib showed drug resistance (Figure S16).

Discussion

In contrast to apoptosis caused by immune silencing, a variety of dangerous signaling molecules and cytokines are activated and released during pyroptosis, accompanied by a strong inflammatory response and activation of the immune system(22). A large number of studies have found that the inflammatory environment can induce the canceration of normal cells, and the inflammatory response environment formed by pyroptosis provides a suitable environment for tumor growth (23). As a ubiquitous death method of tumor cells, pyroptosis has become increasingly prominent in the development of tumors with the deepening of research. However, previous studies on pyroptosis have not identified a prominent role in clinical application, which highlights the significance of pyroptosis-related gene subclasses and prognostic models in predicting the clinical outcomes of glioma patients.

The traditional histologic-based classification has some limitations, although this classification system has been updated several times over the years and serves clinicians well. One of the primary limitations is interobserver variability(24). A previous study reported that the concordance for reviewing a case is only approximately 50% among different neuropathologists, especially for astrocytic glioma versus oligodendroglioma(25). The existing classification criteria may be

inaccurate for cases with mixed tissue features. Prognosis is very different for glioma patients with different subtypes. The lack of understanding of tumor biology could be partly responsible. The development of genomics has allowed us to better understand the differences in prognosis and molecular features and promote effective treatment in glioma subclasses based on molecular features. Using 30 pyroptosis-related genes, we divided glioma patients into two subtypes. Significant overall survival differences were observed between cluster 1 and cluster 2. GSVA indicated that cluster 1 was enriched in some immune-related pathways. We identified 392 DEGs between the two subtypes. GO and KEGG analyses further validated the enrichment of immune-related functions and pathways. Cluster 1 and cluster 2 showed absolute differences in immune cells and immune functions. The infiltration levels of all kinds of immune cells, except Th1 cells, were higher in cluster 1, which had a poor prognosis, than in cluster 2. Cluster 1 also showed more significant trends in some main immune function levels, such as immune checkpoints, inflammation promotion, parainflammation, HLA, T cell and APC inhibition and costimulation, type I and II IFN responses, and cytolytic activity. These results indicated that the classification of glioma based on pyroptosis-related genes was correlated with immune infiltration, which fully reflects the features of strong inflammation and immune response during pyroptosis. A recent study reported that pyroptosis presents antitumor immune function in tumors, namely, pyroptosis-induced inflammation triggers robust antitumor immunity and can synergize with checkpoint blockade(26). Moreover, some key pathways were also highly enriched in cluster 1, such as the NOD-like

receptor signaling pathway, Toll-like receptor signaling pathway, and cytosolic DNA sensing pathway, which were reported to be involved in glioma progression(27-29). Some metabolism-related pathways were also enriched, such as amino sugar and nucleotide, glutathione, glycosaminoglycan and other glycan degradation, and glycosphingolipid biosynthesis. These metabolism-related pathway differences were the main characteristics of glioma classification(30). The differences in clinical features between cluster 1 and cluster 2 were also very evident. IDH status, 1p19q codeletion status, chemotherapy, age, and grade were obviously different. Cluster 1 had more risk components. These results indicated that pyroptosis-related genes divided glioma patients into two-dimensional distributions well. Subsequently, we established a prognostic signature based on 15 pyroptosis-related genes. This prognostic signature was well validated in an external independent cohort. Combining clinical features and the risk score of the 15 genes, we developed a nomogram for clinical application. The CGGA and TCGA datasets showed high consistency. These results indicated that the prognostic signature based on pyroptosis-related genes has high clinical value.

The signature genes were involved in two biological mechanisms of pyroptosis. The assembly of inflammasome bodies is the initial step of the classical pyroptosis pathway. The inflammasome is mainly composed of pattern recognition receptors (PRRs), apoptosis-associated speck-like protein (ASC) and pro-caspase-1 precursors(31). PRRs are receptor proteins responsible for recognizing different signal stimuli in cells. They are mainly composed of nucleotide-binding oligomerization

domain-like receptor protein (NLRP) 1, NLRP3, nucleotide-binding oligomerization domain-like receptor protein C4 (NLRC4), absent in melanoma 2 (AIM2) and other components(32). ASC is an adaptor protein that is mainly composed of the N-terminal pyrindomain (PYD) and the C-terminal caspase activation and recruitment domain (CARD)(33). Procaspase-1 is an effector molecule that can specifically cleave GSDMD after activation. After the danger signal sensor NLR1, NLRP3 or AIM2 recognizes the danger signal molecule, the N-terminal PYD is combined with the N-terminal PYD of the adaptor protein. ASC then recruits Caspase-1 through the interaction of the CARDCARD domain to complete the assembly of the inflamed body(34). This method of cell death mediated by Caspase-1 is called the classical pathway of pyroptosis(35). The nonclassical pathway of pyrolysis is mainly mediated by Caspase-4, Caspase-5 and Caspase-11. After cells are stimulated by bacterial LPS, Caspases-4, -5, and -11 directly bind to bacterial LPS and are activated(36). Activated Caspases-4, -5, and -11 specifically cleave GSDMD and release the intramolecular inhibition of the GSDMD-N domain(37).The GSDMD-N-terminus can activate Caspase-1 by activating the NLRP3 inflammasome(38). Activated Caspase-1 stimulates the maturation of IL-18 and IL-1β precursors, and IL-18 and IL-1β are secreted to the outside of the cell and amplify the inflammatory response. Yang et al found that in the nonclassical pathway that relies on Caspase-11, gap junction protein-1 (Pannexin-1) can be cleaved, and the cleavage of Pannexin-1 can activate its own channel and release ATP, which induces pyrolysis(39). Lamkanfi et al found that in the nonclassical pathway that relies on Caspase-11, Pannexin-1 cleavage can also

activate the NLRP3 inflammasome, which in turn activates Caspase-1 and induces the occurrence of pyroptosis(40). It has been reported that hsa_circ_0001836 knockdown could induce pyroptotic cell death in glioma cells in vitro and in vivo by epigenetically upregulating NLRP1 expression(41). In addition, miR-214 could inhibit cell proliferation and migration through the regulation of pyroptosis mediated by caspase 1 in glioma U87 and T98G cells(42). According to the results, mutations of pyroptosis-related genes are mainly attributed to the classical pathway of pyrolysis. More research is needed to validate the molecular mechanisms.

Based on the risk score, we classified glioma patients into high- and low-risk groups to discriminate clinical outcomes. We further explored the molecular features between the high- and low-risk groups. The functional enrichment analysis results were similar in the TCGA and CGGA datasets, and the same pathways appeared in the two datasets, such as ECM-receptor interaction, GABAergic synapse, focal adhesion, and extracellular matrix organization. The immune cells and immune functions showed similar trends: immune cell and functional scores were higher in the high-risk group. The clinical features showed that cluster 1 had a higher risk score and poorer prognosis than cluster 2. The results indicated that the classification was accurate and validated in the risk model. Furthermore, we compared the gene alterations, CNVs, and DNA methylation levels. Significantly different levels were observed, which reflected the different molecular features of the different risk groups. The ceRNA network identified several key lncRNA-miRNA-mRNA regulatory networks: FAM181A-AS1-miR-21-(CPEB3, SAIB1, BLC7A, MAP2K3, JAG1, TGFBI,

FAM46A, SPRY2, and CALD1). The survival analysis further suggested the regulatory correlation: elevated FAM18A-AS1 and miR-21 were associated with poor prognosis in glioma, and low expression of BCL7A, SATB1 and CPEB3 was associated with favorable prognosis. Previous experiments have reported the promoting role of miR-21 in glioma(43), and upregulation of SATB1 and CPEB3 is associated with the development and progression of glioma(44, 45). The drug sensitivity analysis indicated that NOD2, ELANE, CASP3, and PYCARD showed sensitivity to small molecular drugs, and PRKACA, IL6, and NLLRP3 showed resistance to some drugs. It was reported that the inhibition of the NLRP3 inflammasome by beta-hydroxybutyrate can suppress the migration of glioma cells(46). These results may provide some guidelines for clinical practice.

Currently, our study provides new evidence for glioma classification and prognosis assessment based on pyroptosis-related genes. However, there are still some limitations in the present study. First, the training dataset and validation dataset were from different population settings; the CGGA dataset was from the Chinese population, and the TCGA dataset mainly included Caucasians and some other races. A dataset with a larger sample size is needed to verify the present molecular subtypes. Therefore, it is necessary to validate the prognosis in the subgroup population setting. Finally, in vivo and in vitro experiments are needed to understand the molecular mechanisms and regulatory networks between different subclasses and risk classifications of glioma.

The present study indicated that pyroptosis-related genes can be used to classify

glioma patients into two subclasses based on different molecular features and clinical characteristics. The established prognostic model based on 15 pyroptosis-related genes not only predicted the prognosis of glioma patients but also reflected the molecular alterations, immune infiltration statuses, and stem cell-like properties of different risk groups. The classification based on the risk score of prognostic signature genes revealed a lncRNA-miRNA-mRNA regulatory network. The correlation of signature genes with drug sensitivity may provide a rationale for clinical applications. Finally, our study provides a new understanding of pyroptosis in the development and progression of glioma and contributes new important insights for promoting glioma treatment strategies.

References

1. Weller M, Wick W, Aldape K, *et al.*. Glioma. Nat Rev Dis Primers 2015;1: 15017.

2. Bush NA, Chang SM, Berger MS. Current and future strategies for treatment of glioma. Neurosurg Rev 2017;40: 1-14.

3. Kan LK, Drummond K, Hunn M, Williams D, O'Brien TJ, Monif M. Potential biomarkers and challenges in glioma diagnosis, therapy and prognosis. BMJ Neurol Open 2020;2: e69.

4. Fink SL, Cookson BT. Apoptosis, pyroptosis, and necrosis: mechanistic description of dead and dying eukaryotic cells. Infect Immun 2005;73: 1907-16.

5. Fink SL, Cookson BT. Caspase-1-dependent pore formation during pyroptosis leads to osmotic lysis of infected host macrophages. Cell Microbiol 2006;8: 1812-25.

6. Bergsbaken T, Fink SL, den Hartigh AB, Loomis WP, Cookson BT. Coordinated host responses during pyroptosis: caspase-1-dependent lysosome exocytosis and inflammatory cytokine maturation. J Immunol 2011;187: 2748-54.

7. Boise LH, Collins CM. Salmonella-induced cell death: apoptosis, necrosis or programmed cell death? Trends Microbiol 2001;9: 64-7.

8. Hage C, Hoves S, Strauss L, *et al.*. Sorafenib Induces Pyroptosis in Macrophages and Triggers Natural Killer Cell-Mediated Cytotoxicity Against Hepatocellular Carcinoma. Hepatology 2019;70: 1280-97.

9. Lu C, Guo C, Chen H, *et al.*. A novel chimeric PD1-NKG2D-41BB receptor enhances antitumor activity of NK92 cells against human lung cancer H1299 cells by triggering pyroptosis. Mol Immunol 2020;122: 200-6.

10. An H, Heo JS, Kim P, *et al.*. Tetraarsenic hexoxide enhances generation of mitochondrial ROS to promote pyroptosis by inducing the activation of caspase-3/GSDME in triple-negative breast cancer cells. Cell Death Dis 2021;12: 159.

11. Karki R, Kanneganti TD. Diverging inflammasome signals in tumorigenesis and potential targeting. Nat Rev Cancer 2019;19: 197-214.

12. Xia X, Wang X, Cheng Z, *et al.*. The role of pyroptosis in cancer: pro-cancer or pro-"host"? Cell Death Dis 2019;10: 650.

13. Wang B, Yin Q. AIM2 inflammasome activation and regulation: A structural perspective. J Struct Biol 2017;200: 279-82.

14. Man SM, Kanneganti TD. Regulation of inflammasome activation. Immunol Rev 2015;265: 6-21.

15. Wilkerson MD, Hayes DN. ConsensusClusterPlus: a class discovery tool with confidence assessments and item tracking. Bioinformatics 2010;26: 1572-3.

16. Tang Y, Ye M, Du Y, *et al.*. EGFR signaling upregulates surface expression of the GluN2B-containing NMDA receptor and contributes to long-term potentiation in the hippocampus. Neuroscience 2015;304: 109-21.

17. Suina K, Tsuchihashi K, Yamasaki J, *et al.*. Epidermal growth factor receptor promotes glioma progression by regulating xCT and GluN2B-containing N-methyl-d-aspartate-sensitive glutamate receptor signaling. Cancer Sci 2018;109: 3874-82.

18. Xue Y, Enosi TD, Tan WH, Kay C, Man SM. Emerging Activators and Regulators of Inflammasomes and Pyroptosis. Trends Immunol 2019;40: 1035-52.

19. Fang Y, Tian S, Pan Y, *et al.*. Pyroptosis: A new frontier in cancer. Biomed Pharmacother 2020;121: 109595.

20. Chen R, Smith-Cohn M, Cohen AL, Colman H. Glioma Subclassifications and Their Clinical Significance. Neurotherapeutics 2017;14: 284-97.

21. Coons SW, Johnson PC, Scheithauer BW, Yates AJ, Pearl DK. Improving diagnostic accuracy and interobserver concordance in the classification and grading of primary gliomas. Cancer-Am Cancer Soc 1997;79: 1381-93.

22. Wang Q, Wang Y, Ding J, *et al.*. A bioorthogonal system reveals antitumour immune function of pyroptosis. Nature 2020;579: 421-6.

23. Huang Y, Zhang Q, Lubas M, *et al.*. Synergistic Toll-like Receptor 3/9 Signaling Affects Properties and Impairs Glioma-Promoting Activity of Microglia. J Neurosci

2020;40: 6428-43.

24. Saxena S, Jha S. Role of NOD- like Receptors in Glioma Angiogenesis: Insights into future therapeutic interventions. Cytokine Growth Factor Rev 2017;34: 15-26.

25. Giurdanella G, Motta C, Muriana S, *et al.*. Cytosolic and calcium-independent phospholipase A(2) mediate glioma-enhanced proangiogenic activity of brain endothelial cells. Microvasc Res 2011;81: 1-17.

26. Woolf EC, Scheck AC. Metabolism and glioma therapy. CNS Oncol 2012;1: 7-10.

27. Platnich JM, Muruve DA. NOD-like receptors and inflammasomes: A review of their canonical and non-canonical signaling pathways. Arch Biochem Biophys 2019;670: 4-14.

28. Man SM, Kanneganti TD. Regulation of inflammasome activation. Immunol Rev 2015;265: 6-21.

29. Nambayan R, Sandin SI, Quint DA, Satyadi DM, de Alba E. The inflammasome adapter ASC assembles into filaments with integral participation of its two Death Domains, PYD and CARD. J Biol Chem 2019;294: 439-52.

30. Lu A, Magupalli VG, Ruan J, *et al.*. Unified polymerization mechanism for the assembly of ASC-dependent inflammasomes. Cell 2014;156: 1193-206.

31. Case CL, Roy CR. Analyzing caspase-1 activation during Legionella pneumophila infection in macrophages. Methods Mol Biol 2013;954: 479-91.

32. Lagrange B, Benaoudia S, Wallet P, *et al.*. Human caspase-4 detects tetra-acylated LPS and cytosolic Francisella and functions differently from murine

caspase-11. Nat Commun 2018;9: 242.

33. Shi J, Zhao Y, Wang K, *et al.*. Cleavage of GSDMD by inflammatory caspases determines pyroptotic cell death. Nature 2015;526: 660-5.

34. Kayagaki N, Stowe IB, Lee BL, *et al.*. Caspase-11 cleaves gasdermin D for non-canonical inflammasome signalling. Nature 2015;526: 666-71.

35. Yang D, He Y, Munoz-Planillo R, Liu Q, Nunez G. Caspase-11 Requires the Pannexin-1 Channel and the Purinergic P2X7 Pore to Mediate Pyroptosis and Endotoxic Shock. Immunity 2015;43: 923-32.

36. Lamkanfi M, Dixit VM. Mechanisms and functions of inflammasomes. Cell 2014;157: 1013-22.

37. Jiang Z, Yao L, Ma H, *et al.*. miRNA-214 Inhibits Cellular Proliferation and Migration in Glioma Cells Targeting Caspase 1 Involved in Pyroptosis. Oncol Res 2017;25: 1009-19.

38. Liu Y, Wu H, Jing J, Li H, Dong S, Meng Q. Downregulation of hsa_circ_0001836 Induces Pyroptosis Cell Death in Glioma Cells via Epigenetically Upregulating NLRP1. Front Oncol 2021;11: 622727.

39. Hermansen SK, Nielsen BS, Aaberg-Jessen C, Kristensen BW. miR-21 Is Linked to Glioma Angiogenesis: A Co-Localization Study. J Histochem Cytochem 2016;64: 138-48.

40. Chu SH, Ma YB, Feng DF, *et al.*. Upregulation of SATB1 is associated with the development and progression of glioma. J Transl Med 2012;10: 149.

41. He Y, Nan H, Yan L, *et al.*. Long non-coding RNA MIR22HG inhibits glioma

progression by downregulating microRNA-9/CPEB3. Oncol Lett 2021;21: 157.

42. Shang S, Wang L, Zhang Y, Lu H, Lu X. The Beta-Hydroxybutyrate Suppresses the Migration of Glioma Cells by Inhibition of NLRP3 Inflammasome. Cell Mol Neurobiol 2018;38: 1479-89.

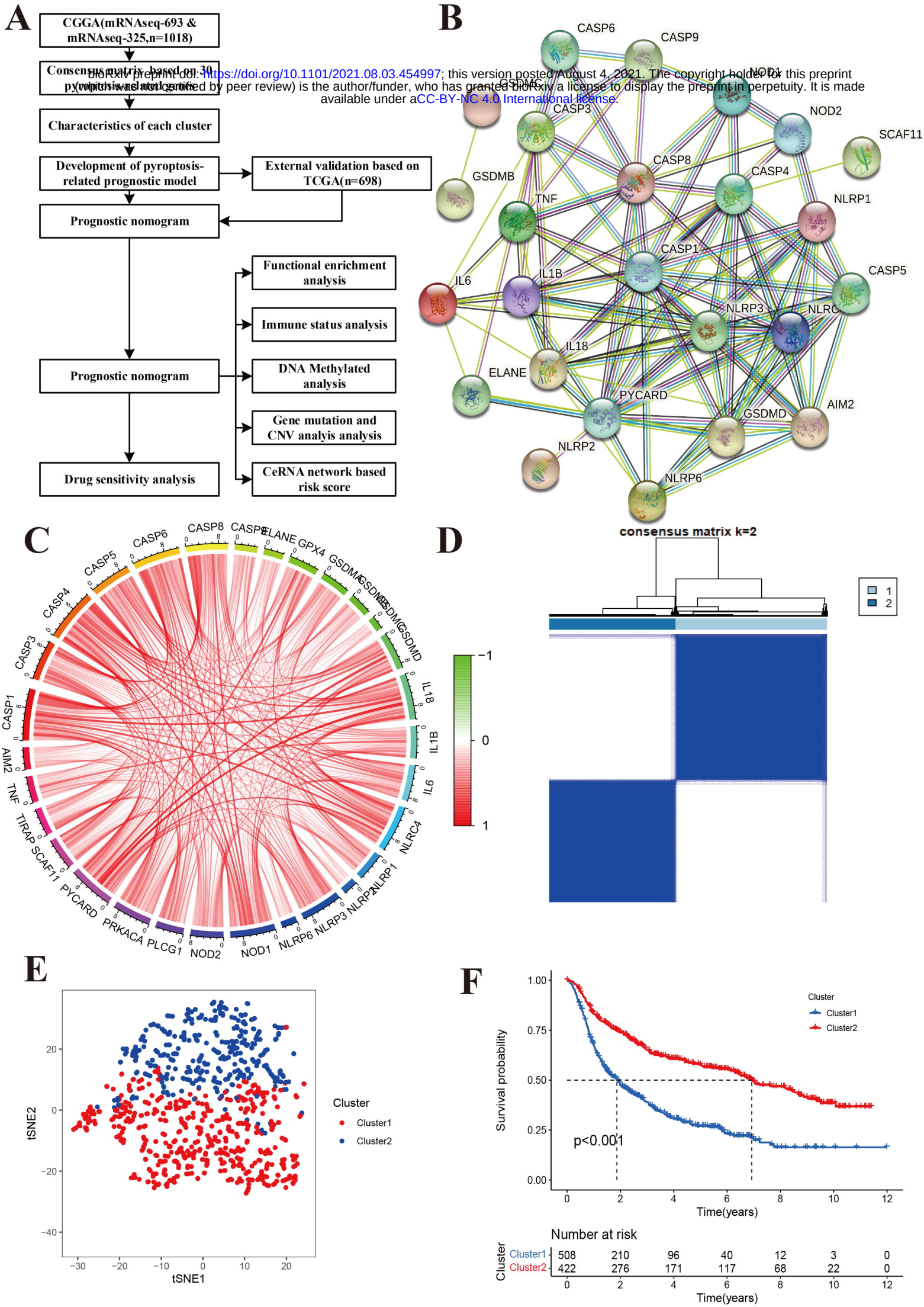

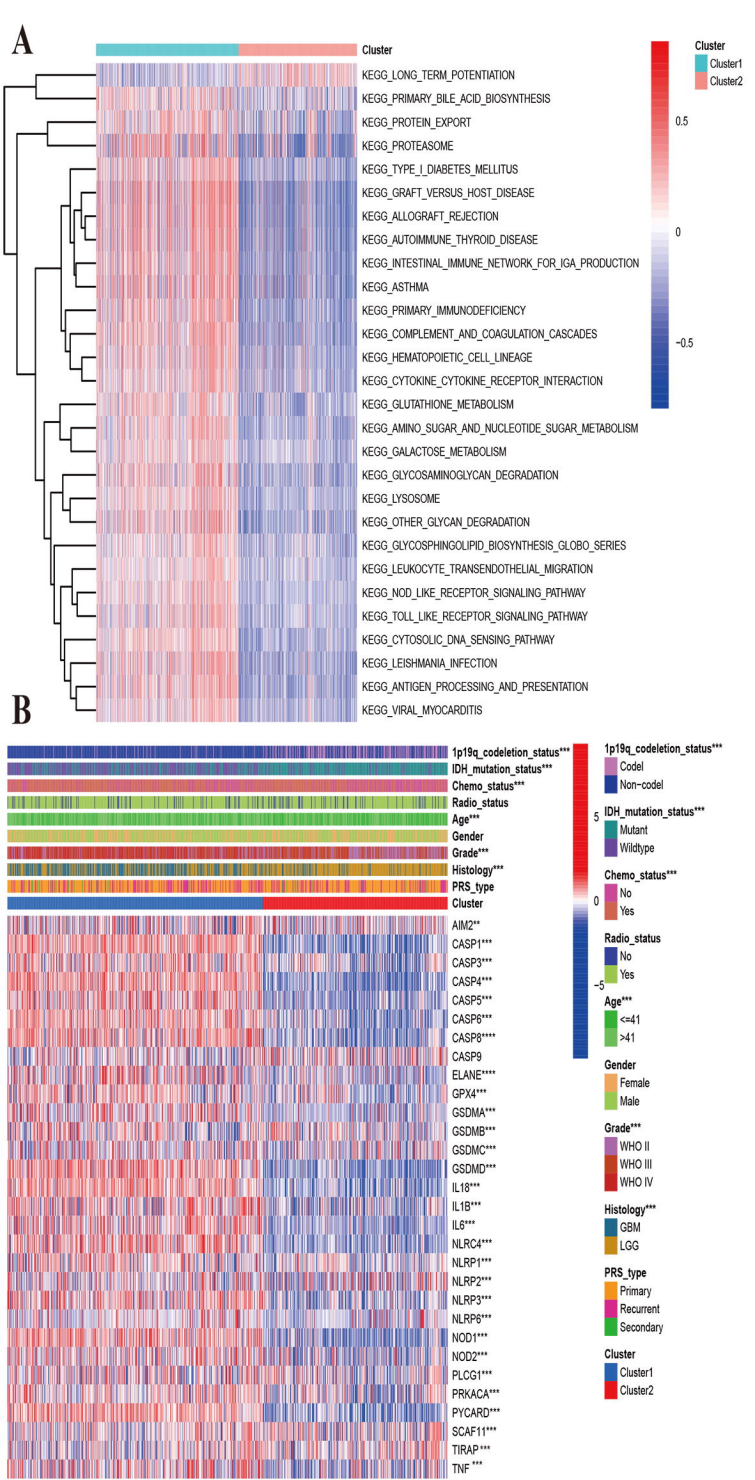
A
Cluster
KEGG_LONG_TERM_POTENTIATION
KEGG_PRIMARY_BILE_ACID_BIOSYNTHESIS
KEGG_PROTEIN_EXPORT
KEGG_PROTEASOME
KEGG_TYPE_I_DIABETES_MELLITUS
KEGG_GRAFT_VERSUS_HOST_DISEASE
KEGG_ALLOGRAFT_REJECTION
KEGG_AUTOIMMUNE_THYROID_DISEASE
KEGG_INTESTINAL_IMMUNE_NETWORK_FOR_IGA_PRODUCTION
KEGG_ASTHMA
KEGG_PRIMARY_IMMUNODEFICIENCY
KEGG_COMPLEMENT_AND_COAGULATION_CASCADES
KEGG_HEMATOPOIETIC_CELL_LINEAGE
KEGG_CYTOKINE_CYTOKINE_RECEPTOR_INTERACTION
KEGG_GLUTATHIONE_METABOLISM
KEGG_AMINO_SUGAR_AND_NUCLEOTIDE_SUGAR_METABOLISM
KEGG_GALACTOSE_METABOLISM
KEGG_GLYCOSAMINOGLYCAN_DEGRADATION
KEGG_LYSOSOME
KEGG_OTHER_GLYCAN_DEGRADATION
KEGG_GLYCOSPHINGOLIPID_BIOSYNTHESIS_GLOBO_SERIES
KEGG_LEUKOCYTE_TRANSENDOTHELIAL_MIGRATION
KEGG_NOD_LIKE_RECEPTOR_SIGNALING_PATHWAY
KEGG_TOLL_LIKE_RECEPTOR_SIGNALING_PATHWAY
KEGG_CYTOSOLIC_DNA_SENSING_PATHWAY
KEGG_LEISHMANIA_INFECTION
KEGG_ANTIGEN_PROCESSING_AND_PRESENTATION
KEGG_VIRAL_MYOCARDITIS
Cluster
Cluster1
Cluster2
0.5
0
−0.5
B
1p19q_codeletion_status***
IDH_mutation_status***
Chemo_status***
Radio_status
Age***
Gender
Grade***
Histology***
PRS_type
Cluster
AIM2**
CASP1***
CASP3***
CASP4***
CASP5***
CASP6***
CASP8****
CASP9
ELANE****
GPX4***
GSDMA***
GSDMB***
GSDMC***
GSDMD***
IL18***
IL1B***
IL6***
NLRC4***
NLRP1***
NLRP2***
NLRP3***
NLRP6***
NOD1***
NOD2***
PLCG1***
PRKACA***
PYCARD***
SCAF11***
TIRAP***
TNF***
5
0
−5
1p19q_codeletion_status***
Codel
Non−codel
IDH_mutation_status***
Mutant
Wildtype
Chemo_status***
No
Yes
Radio_status
No
Yes
Age***
<=41
>41
Gender
Female
Male
Grade***
WHO II
WHO III
WHO IV
Histology***
GBM
LGG
PRS_type
Primary
Recurrent
Secondary
Cluster
Cluster1
Cluster2

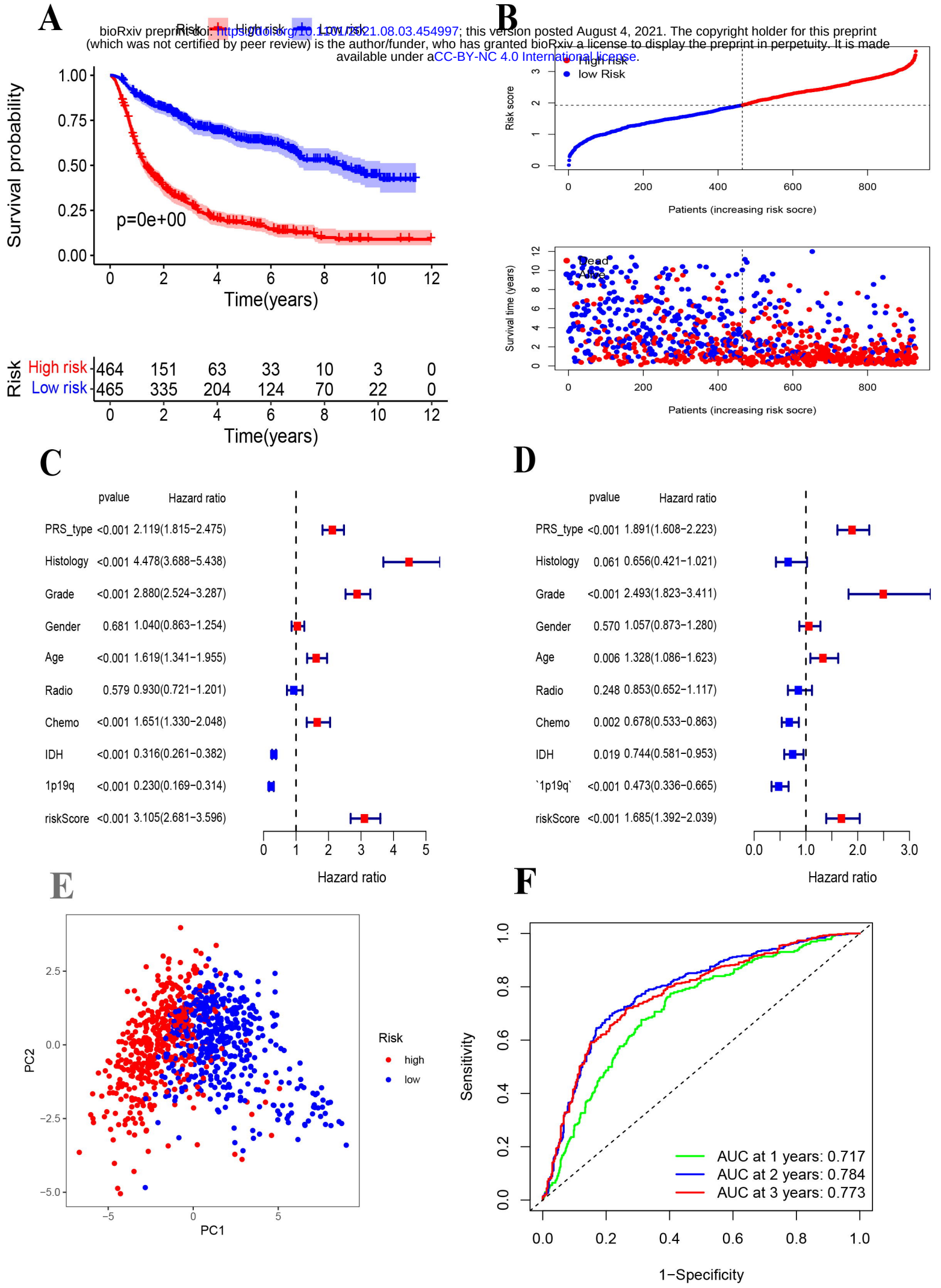

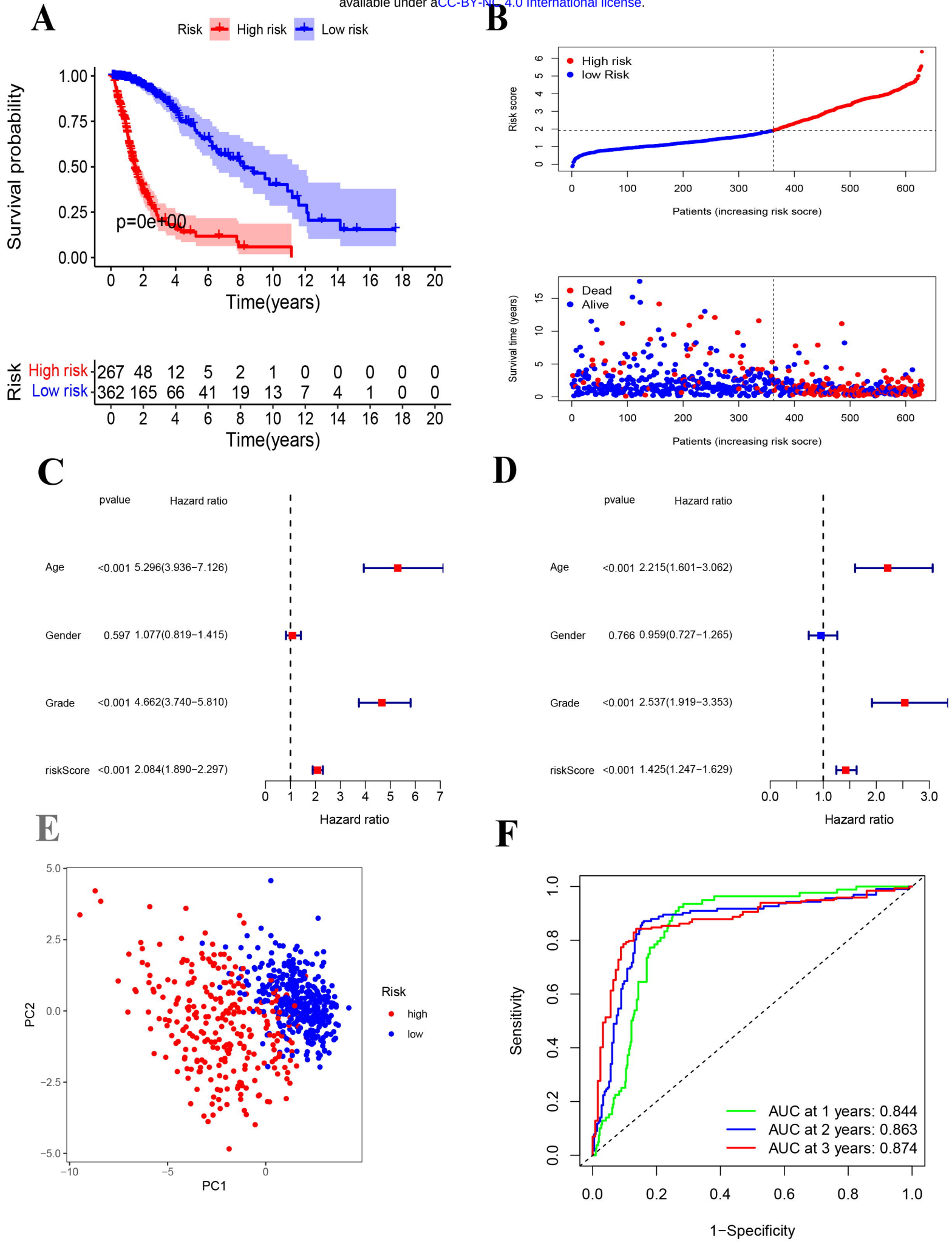

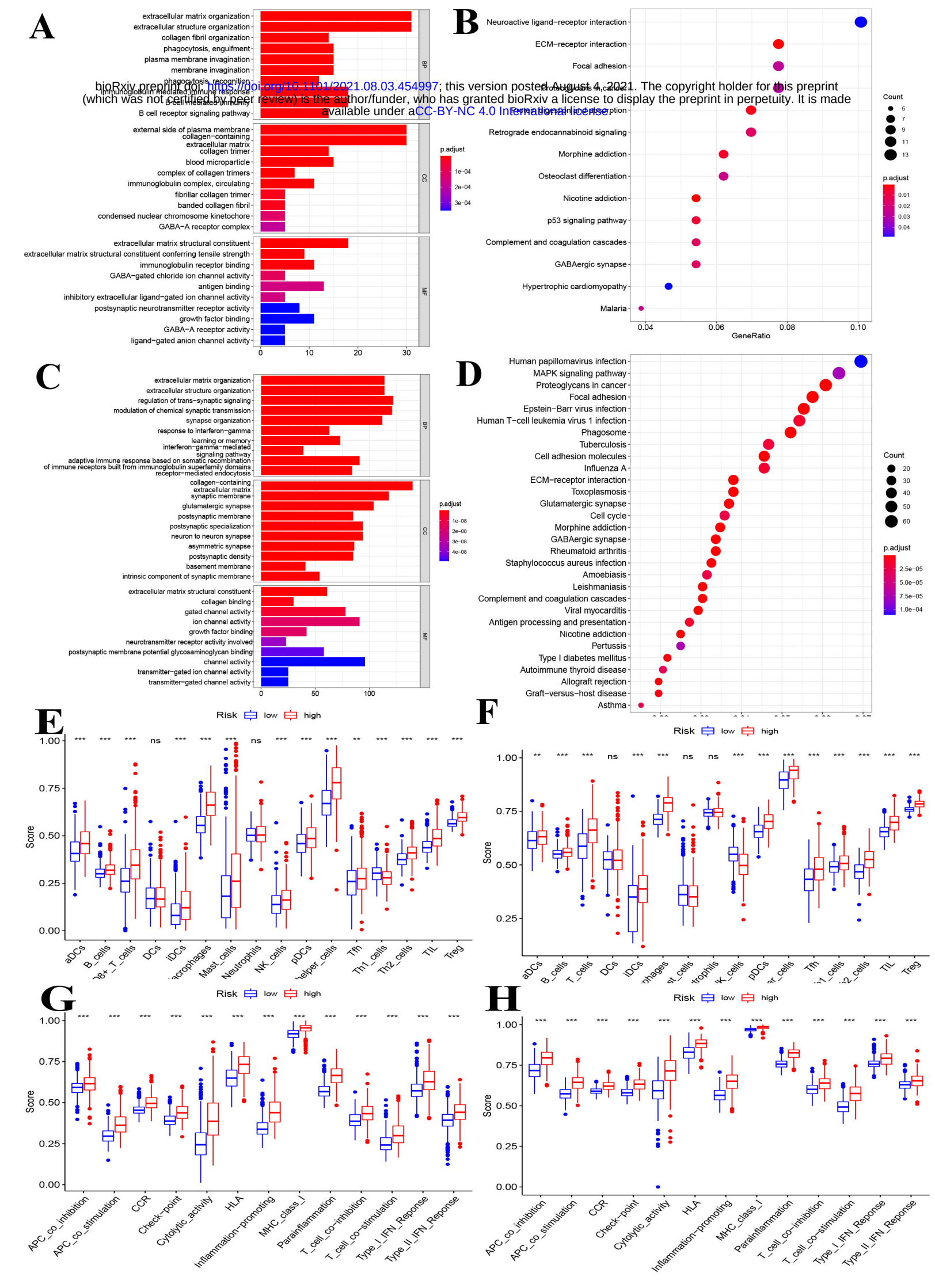

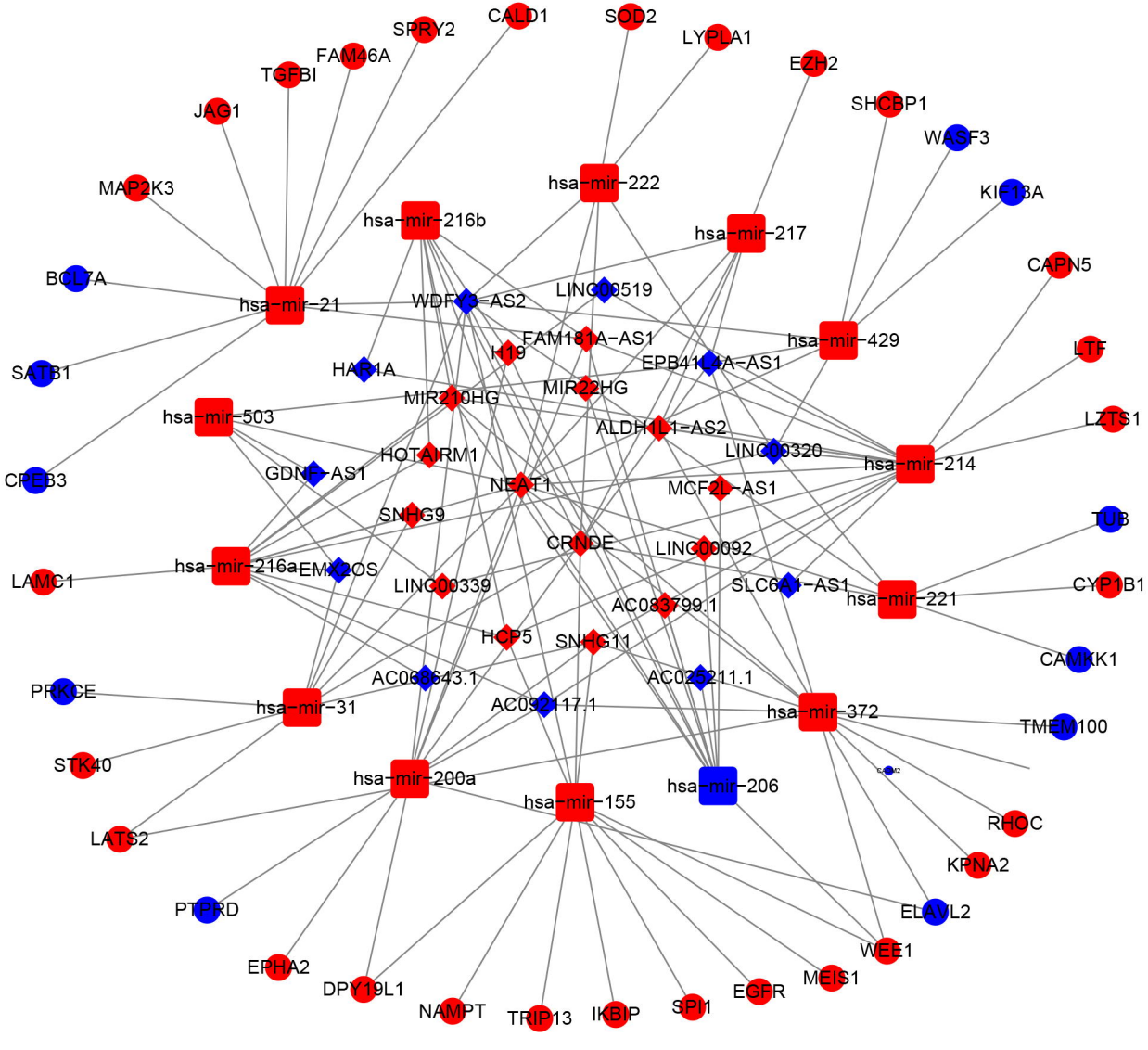
CALD1
SOD2
SPRY2
LYPLA1
FAM46A
TGFBI
EZH2
JAG1
SHCBP1
WASF3
MAP2K3
hsa-mir-222
KIF18A
hsa-mir-216b
hsa-mir-217
CAPN5
BCL7A
hsa-mir-21
WDFY3-AS2
LINC00519
FAM181A-AS1
hsa-mir-429
LTF
H19
SATB1
HAR1A
EPB41L4A-AS1
MIR210HG
MIR22HG
hsa-mir-503
LZTS1
ALDH1L1-AS2
HOTAIRM1
LINC00320
CPEB3
GDNF-AS1
hsa-mir-214
NEAT1
MCF2L-AS1
SNHG9
TUB
CRNDE
hsa-mir-216a
LINC00092
LAMC1
EMX2OS
LINC00339
SLC6A1-AS1
CYP1B1
AC083799.1
hsa-mir-221
HCP5
SNHG11
CAMKK1
AC068643.1
AC025211.1
PRKCE
hsa-mir-31
AC092117.1
hsa-mir-372
TMEM100
STK40
hsa-mir-200a
hsa-mir-206
hsa-mir-155
RHOC
LATS2
KPNA2
PTPRD
ELAVL2
WEE1
EPHA2
MEIS1
DPY19L1
EGFR
NAMPT
TRIP13
IKBIP
SPI1